An experiment on full-day power generation building fabric component for zero-energy buildings

Jingming Li[a], Nianping Li[a, *], Meng Wang[a]

[a]College of Civil Engineering, Hunan University, Changsha 410082, China

Abstract

Thermal electricity generation (TEG) is a potential method to utilize energy emitted from the built environment. This work presents a prototype of the low-cost full-day power generation solar building component, which can be integrated as the building fabric or as a part of the solar panels. The size of the prototype is 0.04 m^2. The overall cost is less than 25 USD. The prototype is tested in various environments to validate its performance. The first experiment tests its performance under the radiation of a high-temperature source, the prototype can generate the highest voltage of 0.8 V. In onsite experiments, it can reach a maximum value of 10 mW/m^2 under sunlight. It can also work at night depending on the thermal radiation of the environment. It can also be used in different weather; the performance is even better than the nighttime. The experiments indicate that radiation heat transfer has a stronger influence on energy conversion than the convective heat transfer. The relative humidity has a certain influence on its performance, but there is no obvious effect of radiation heat transfer. Although the prototype has great potential, there are still limitations, and this article also discusses the problems. Meanwhile, this article also points out possible directions for improving design in the future. The results in this article might be helpful for zero-energy buildings and low-carbon buildings.

Keywords: Thermal electricity generation; Full day power generation; Solar building

1. Introduction

Energy is an important material foundation for social development and an economic driving force. Energy use in the building sector involves multiple stages of design, construction, operation, and demolition, and most of its energy consumption occurs during the construction and operation stages. The final energy consumption of global buildings in 2018 increased by 1% compared to 2017 and has increased by 8 EJ since 2010 [1]. The massive increase in energy consumption in the building sector is since the growth of building area and population has surpassed the increase in energy efficiency, and the

growth of the building area far exceeds energy demand. In terms of carbon emission, the Architecture, Engineering, and Construction (AEC) Industry is also a major carbon emitter. The global construction industry status report shows that the global construction industry-related energy consumption accounts for 36% of the world, and the construction sector's carbon emissions reach 11Gt, accounting for 39% of the world, of which 11% comes from the production of construction materials such as steel, cement, and glass [2]. In 2018, the building area increased by 3% compared with 2017, which is a cumulative increase of 23% since 2010. By 2050, as the global population increases by 2.5 billion, new buildings will have an important impact on future energy use and emissions associated with buildings [1].

Consequently, renewable energy and zero-energy buildings are in the ascendant. Solar energy, wind energy, and other renewable technologies gained massive investments. By 2017, renewable sources provided about 18% of the world's energy supply [3]. Among them, building solar energy harvesting systems are increasingly common[4,5], due to its advantage of utilizing the building exterior structures for electricity generation.

TEG applications on waste heat as the renewable energy source emerged [6]. There are studies [7,8] designing a system to reuse waste heat from coalfield subsurface fires. The system was mainly heat recovery; the electric heat conversion efficiency was not ideal. To improve thermoelectric conversion efficiency, Ye et al. [9] designed multi-stage waste heat recovery to harvest heat from ship chimneys. Al-Nimr et al. [10] used TEG to harvest solar energy and to produce distilled water at the same time. In addition to natural heat transfer, there are also studies on the use of industrial waste heat. Chiarotti et al. [11] designed a smaller power prototype to recover heat from industrial water. Cheng et al. [12] developed a 1.2 kW TEG project by using industrial waste heat. Following similar purposes, Abbasi and Tabar [13] measured the vehicles' waste energy and attached TEG units to the exhaust for energy harvesting. García-Contreras et al. [14] validated TEG energy conversion performance from exhaust gases.

The temperature differences of TEG applications is constantly decreasing, from coalfield subsurface fires to the human body. A quantitative study measured the power output converted from the human body and concluded that the forehead was the maximum source for energy conversion [15]. Elmoughni et al. [16] integrated TEG into textiles for body heat harvesting, and the output was about 47 mV. Hyland et al. [17] tested a flexible TEG T-shirt and compared its performance on different body locations with experiments. By the time Yuan and Zhu [18] applied flexible TEG for powering wearable devices from body heat, the

output power had reached 4.95 mW. Although the human body's heat production does not reach the high-temperature difference in the industry, it also has stable power output. These works further expand the potential of TEG working in a low-temperature difference environment.

With the development of technology and process, TEG can provide power during nighttime through heat transfer. The reviews [19,20] summarized the application of TEG in walls, and its primary function was for heat recovery from PV panels. Also, PV-TEG integration in walls can improve the thermal performance [19]. The use of TEG can effectively make up for building-integrated solar systems' problems of power generation during the night. The building envelope can not only provide conditions for radiation heat exchange in the night sky but also has long-term radiation heat exchange with the surrounding environment, which can provide a stable source of thermoelectric conversion for TEG. Recently, Fan et al. [21] reached more than 2 W/m^2 via a vacuum chamber connected with radiative cooling, while the cost is much higher than previous studies. Technological progress has allowed TEG to have more applications in buildings. Aksamija et al. [22] integrated TEG with building facade systems and tested its performance under different temperatures from -18 °C to 32 °C. Their study proved the application of TEG in building facade systems under experimental environments.

Meanwhile, although TEG has gradually been widely used in buildings, its cost is still not low, and the TEG of the building maintenance structure in the past research is embedded in the wall, there are difficulties in maintenance and replacement, so it is necessary to reduce costs and provide flexible maintenance plan. In recent years, Raman et al. [23] powered a LED using night sky radiation with TEG units of 0.04 m^2 for about 30 USD. To utilize the advantage of TEG and lower the cost, this study presented a prototype of a full-day electricity building fabric component using TEG. It can be integrated into the façade systems or installed as exterior shading. The design of the component is explained. The component was tested in an experiential environment to assess its peak performance. A field test is conducted later to understand its on-site performance. After assessing the performances of the full day power generation component, the limitations and suggestions are discussed for optimizing the design.

2. Methodology

The section explains the structure of the full day power generation solar building component, experimental conditions, and devices used for the tests.

2.1. The structure of the component

The component has five layers, which are consist of aluminum heatsinks, aluminum plate, thermal grease, TEG units, polyethylene aluminum foil, and polyethylene aluminum foil, as shown in Figure 1.

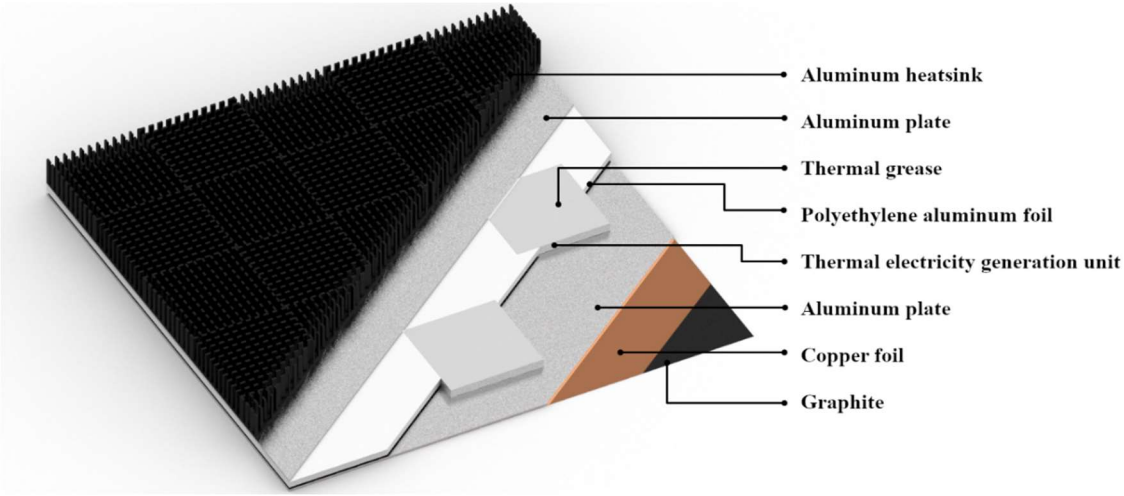

Fig. 1. The structure of the full day power generation solar building component.

The aluminum heatsinks, with thermal conductivity of 209 W/(m*K), are to increase the area for heat transfer. The aluminum plate, with thermal conductivity of 237 W/(m*K), is to stick the heatsinks and to connect the TEG units. The thermal grease, on both sides of the TEG units, is to enhance heat transfer. The TEG unit has an internal resistance of 2 Ω. The thermal isolation layer used polyethylene aluminum foil, is to make sure heat transfer only goes through the TEG units. The graphite copper foil layer, with a vertical thermal conductivity of 600 W/(m*K), is to enhance heat transfer. The parameters of the layers are listed in Table 1. The prototype is inserted into a 5 cm Expand Aple Poly Ephylene framework as shown in Figure 2.

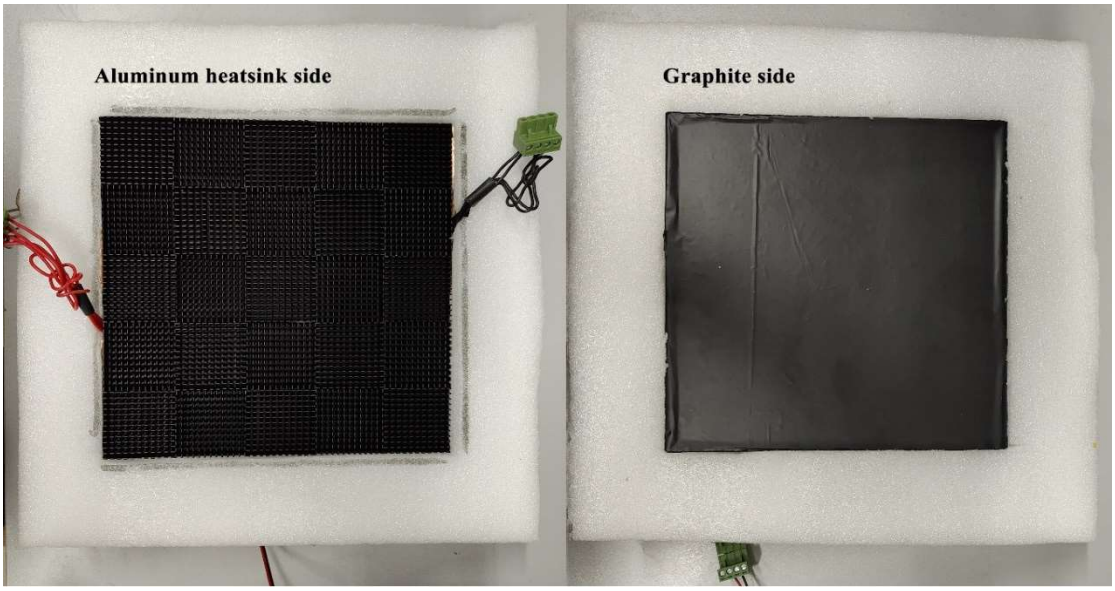

Fig. 2. The prototype of the component

Table 1

The parameters of the layers in the component.

Name	Size	Amount
Graphite copper foil	0.05*200*200 mm	1
Aluminum heatsink	40*40*11 mm	25
Aluminum plate	200*200*0.5 mm	2
TEG unit	40*40*3.8 mm	4

2.2. The theoretical model of the prototype

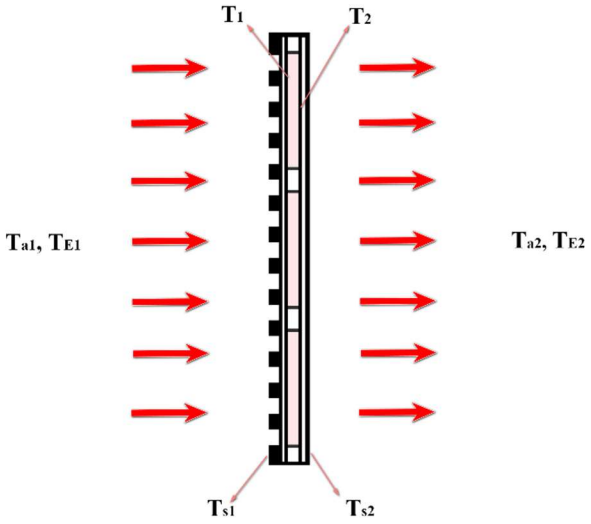

Fig. 3. The theoretical working conditions of the prototype.

When the layers are connected, the prototype could convert heat transfer to electricity. The working conditions are as shown in Figure 3. Assuming the air temperature is T_{a1} and the environment temperature is T_{E1}, the heat convection on the aluminum heatsink side is Q_{C1}, and the radiation heat transfer is Q_{R1}, Q_{C1} and Q_{R1} can be calculated with Equation (1) and (2). The heat conduction between the aluminum heatsink and the TEG units can be calculated through Equation (3).

$$Q_{C1} = h \times (T_{E1} - T_{s1}) \times A \quad (1)$$

$$Q_{R1} = C_1 \times \left(\left(\frac{T_{E1}}{100}\right)^4 - \left(\frac{T_{s1}}{100}\right)^4\right) \quad (2)$$

$$q = \lambda \times (T_{s1} - T_1) \times A \quad (3)$$

Where h is the convective heat transfer coefficient, A is the surface area, C_1 is the surface radiant heat transfer coefficient, and λ is the thermal conductivity. Similarly, Q_{C2}, Q_{R2}, and q_1 on the graphite copper foil can be calculated.

$$W_{max}^{\cdot} = \frac{S^2(T_1 - T_2)^2}{4R} \quad (4)$$

The electricity generated from the TEG units can be calculated with Equation (4) [24,25], where S is the Seebeck coefficient. Since q equals to the sum of the amount of radiation and convection, the connection of electricity generated by the prototype and the environmental temperature can be computed through Equation (1), (2), (3), and (4).

2.3. Tests in the various environments

The component is firstly tested indoor with a radiative heater and then tested on-site. Table 2 illustrates the devices used in the experiments.

Table 2

The Devices in the experiments.

Device	Parameters
MDN-RT605 radiative heater	600 W
UT71A digital multimeters	Maximum Precision (mV): ± (0.1%+8)
UT71D digital multimeters	Maximum Precision (V): ± (0.05%+5)
	Maximum Precision (mA): ± (0.15%+15)
RS-WS-WIFI-6 thermo-hygrometer	Relative Humidity: ± 3%
	Temperature (K): ± 0.5
FLIR C3 thermal camera	Temperature (K): ±2

The indoor temperature is maintained at 299.15 K, relative humidity is around 80%. The straight-line distance between the component and the radiative heater is 52 cm as shown in Figure 4. UT71D is used to measure the voltage and current during this phase. A thermal camera is used to measure the temperatures.

The outdoor experiment was conducted in a three-story building in Changsha. The site environment is shown in Figure 5, the location is in red. The location is surrounded by trees and other buildings. The experiment lasted six days, from August 19th to 25th. The sunlight simulation, run by Ladybug using the weather file of Changsha, indicated the location could have 40-72 hours of sunshine.

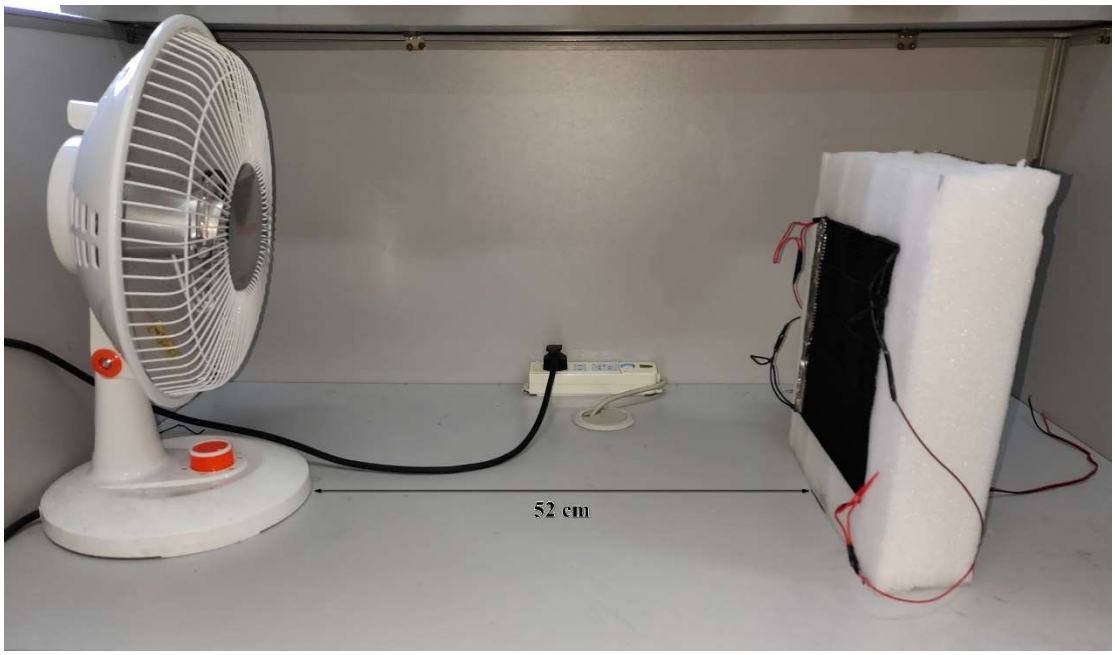

Fig. 4. The layout of the indoor experiment.

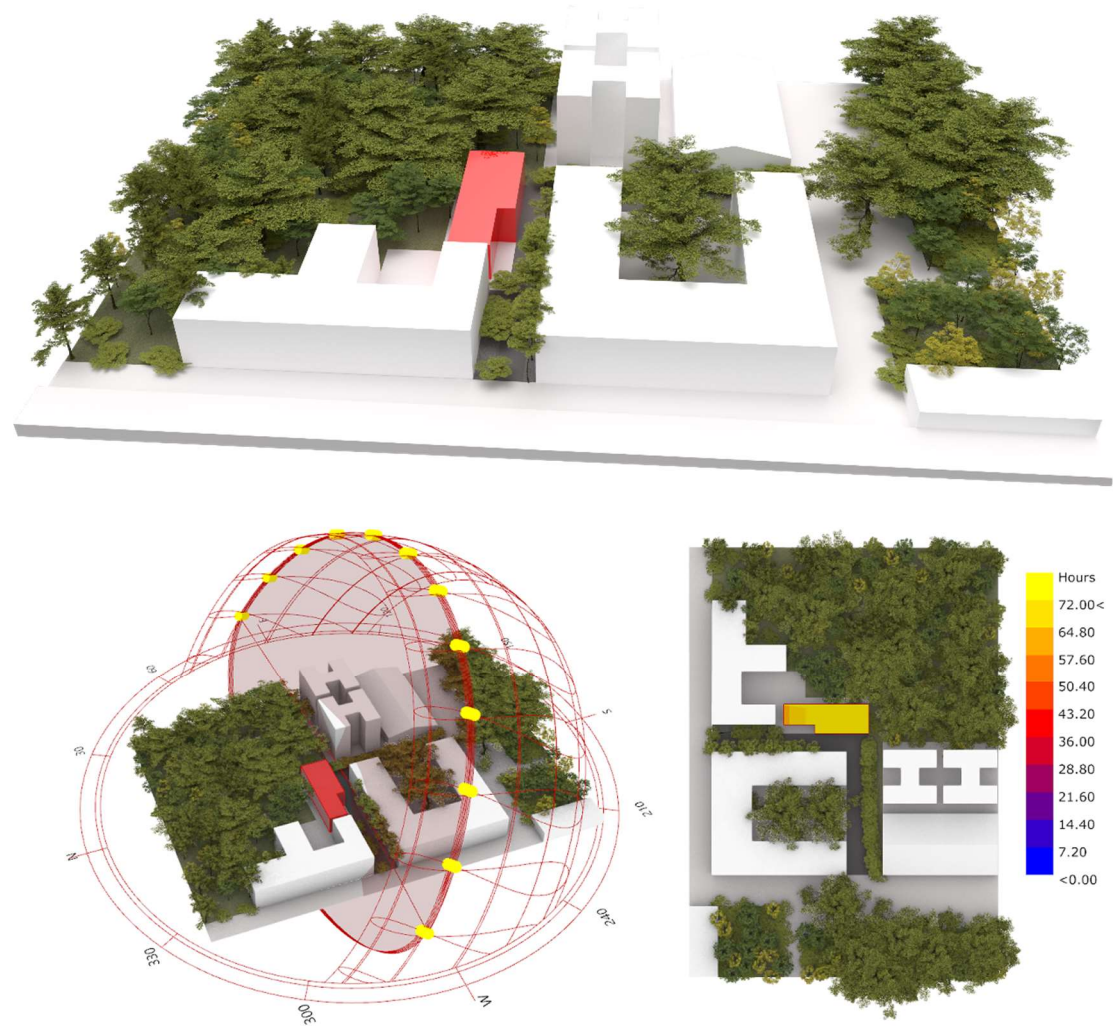

Fig. 5. The site of the outdoor experiment.

The prototype is placed 5cm from a window of the building, which is about 7 meters above the ground. In the first three days, the aluminum heatsinks are facing outside. The graphite copper foil is facing outside in the following three days. A thermo-hygrometer is placed by the side of the prototype, another is placed indoor by the window. Two laptops are used to connect the multimeters for data logging. The collected data are processed and plotted with Matplotlib.

Fig. 6. The position of the component during the outdoor experiment.

3. Findings

The indoor experiment tested its power generation ability under radiation as shown in Figure 7. The heat source could reach 453 K when working.

The results are plotted in Figure 8. During the first 180 seconds when the radiative heater is offline, the prototype could a voltage of about 0.03 V due to the differences in convective heat transfer coefficient on both sides, the heat transfer flows from the aluminum heatsinks to the graphite side. When the heater is working, affected by radiation, the heat flow reverses and the value of voltage increases increasingly fast. The highest voltage could reach 0.8 V under the radiation of the high-temperature source. The temperature difference between the two sides of the sample plate gradually decreases, and the heat

conduction gradually decreases. When the voltage reaches the maximum value, the voltage gradually decreases, and the rate of decrease becomes slower and slower. After 4000 seconds, the voltage stabilizes at 0.51 V to 0.52 V.

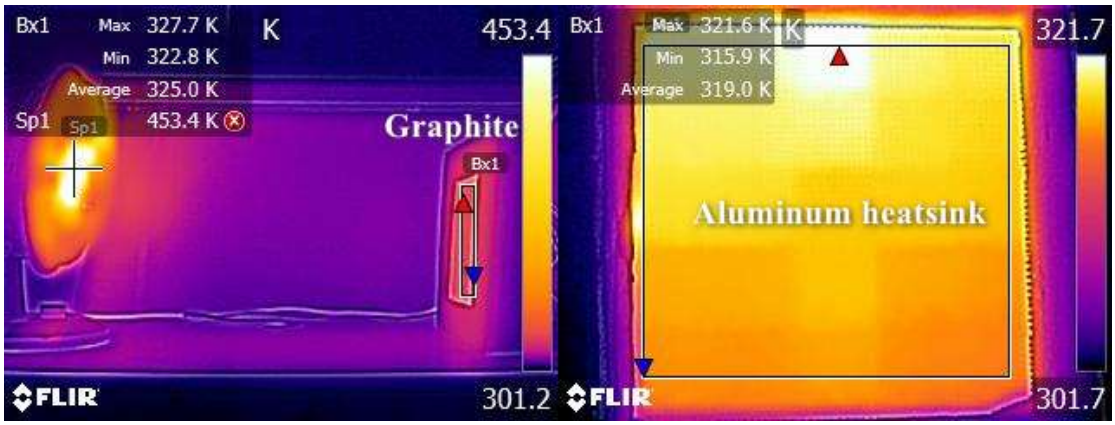

Fig. 7. Thermal performance of the prototype during the indoor test.

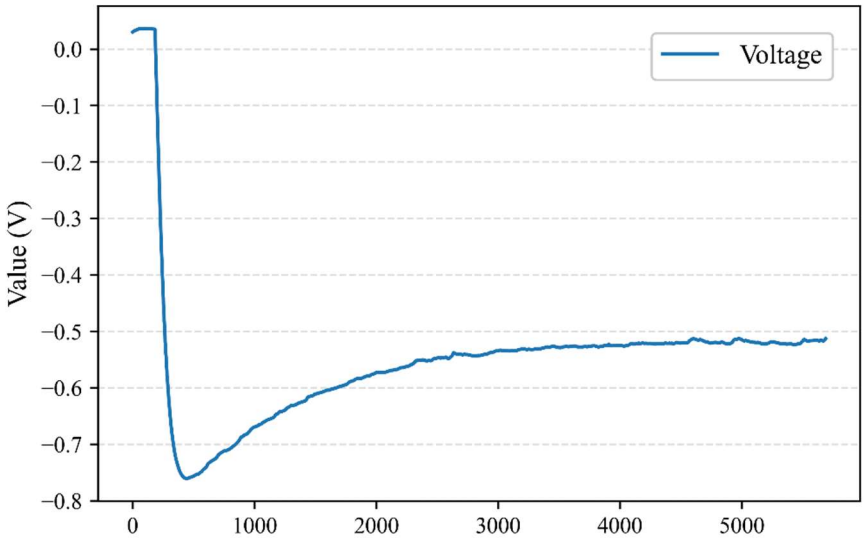

Fig. 8. The voltage generated by the prototype during the indoor test.

Thereafter, the prototype is placed at the position as shown in Figure 6. The aluminum heatsinks were facing outside in the first three days. The performance and surrounding environments are plotted in Figure 9. Voltage and current reached the maximum values in the daytime. The voltage could reach 30 mV to 35 mV, and the current could reach 5 mA to 7mA. The reason for the steep rise and fall of the curve in the image is the influence of solar radiation. When the indoor temperature is higher than the outdoor temperature, the prototype can absorb the indoor heat radiation to generate extremely low voltage power. Figure 10 demonstrates the performance during the following three days when the graphite copper

foil was facing outside. The changes in thermoelectric conversion are the same. The higher conversion volume on August 25 may be due to the increase in the temperature difference between indoor and outdoor caused by rainfall.

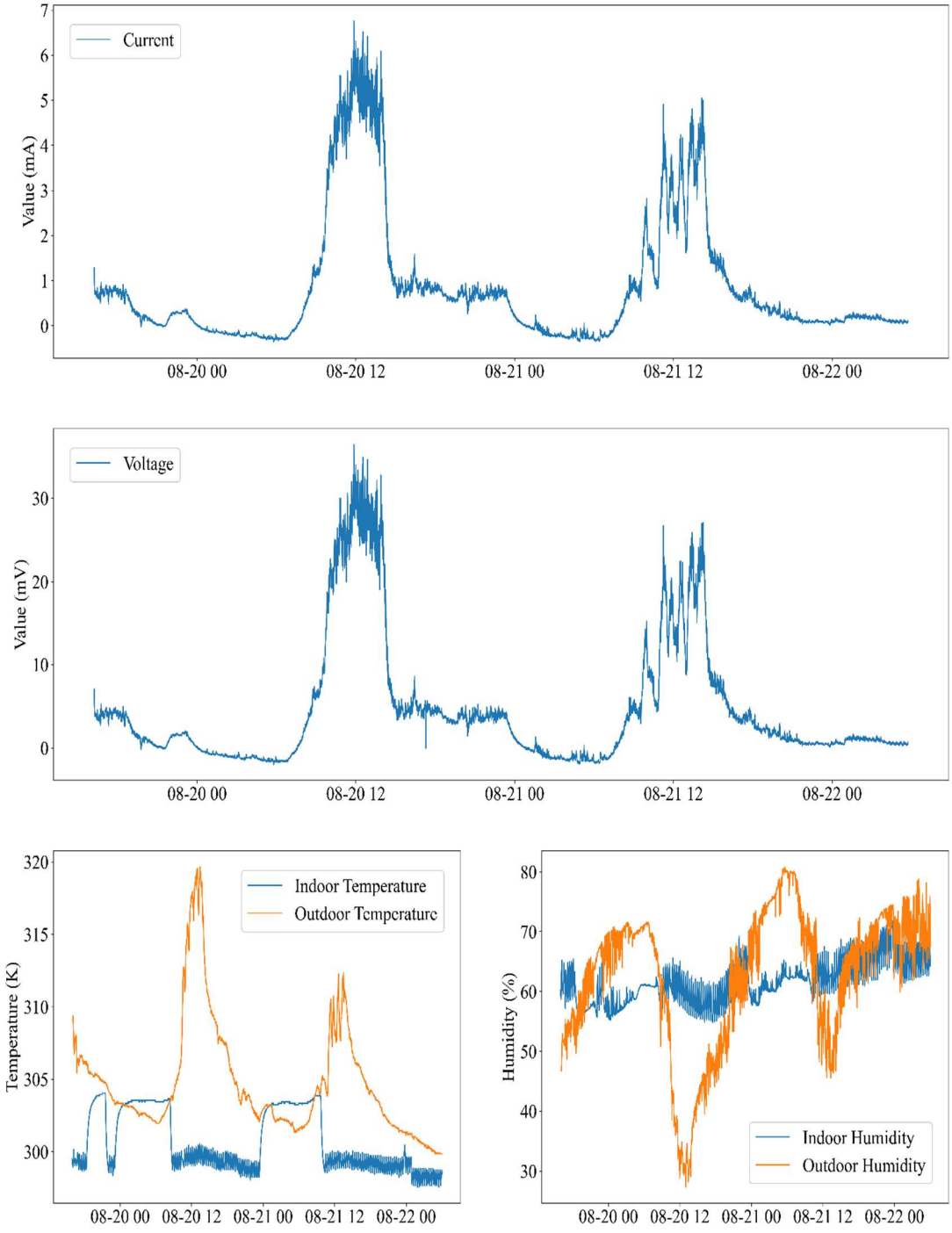

Fig. 9. Performance of the prototype when the aluminum heatsinks facing outside.

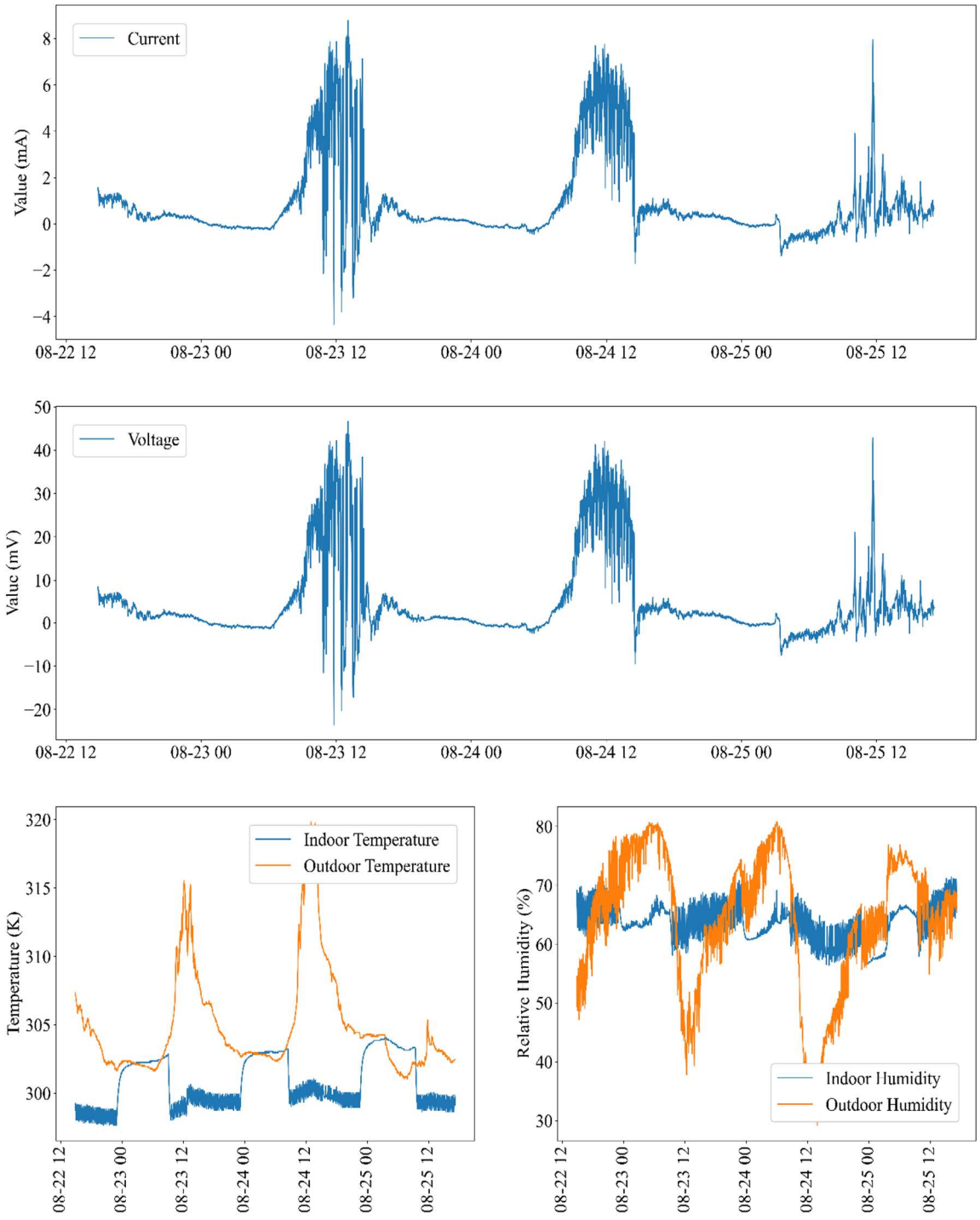

Fig. 10. Performance of the prototype when the graphite facing outside.

4. Discussions

The section discussed the parameters affecting the performance of the prototype. The limitations and the possible methods to improve the performance are also included.

4.1. Key factors on the performance

The materials are the basics. The differences in the radiant heat transfer coefficient, convective heat transfer coefficient, and the heat capacity make the prototype produce a stable temperature difference on both sides, which can be converted into electrical energy

Solar radiation has a great impact on performance. Due to the black surface, when the graphite side faces outward, the effects of radiative heat transfer is obvious considering the curve in Figure 8. Comparing Figure 9 and Figure 10, voltage fluctuations when the graphite is facing outside are particularly severe. Since the radiation and convection of the graphite copper foil are much higher than the other side, when there is solar radiation on the graphite, the heat transfer of graphite copper foil accelerates, and the voltage rises. When the clouds block the sunlight, the graphite copper foil dissipates heat quickly, and the voltage increases rapidly in the other direction.

Environmental temperatures also have influences on performance. Although it is not obvious during the day when the indoor temperature at night is higher than the outdoor temperature, the prototype can still convert part of the radiant heat exchange into electricity relative humidity may also influence the performance. The rainfall on August 25 caused a higher conversion volume at nighttime. The increase might be caused by relative humidity and temperature change considering the curve changes in Figure 10.

4.2. Limitations

The experiments have proved the usability of the prototype. However, there are still some limitations. Generally, the power generated by the 0.04 m^2 prototype is low, the maximum value is only 10 mW/m^2, which is much lower than the power in [21,23], even though the environments are different. Secondly, the prototype did not have an external protective layer, meaning that the winds could affect heat convention. Because of the area of the prototype, whether the effects of wind could increase or decrease electricity generation has not been studied in-depth in this work. Meanwhile, the temperatures of both sides of the prototype are not measured, due to the limit of the prototype's area and the measuring instruments. Also, the structure of the device needs to be enhanced. The prototype could generate over 1 V during indoor tests when first assembled. However, because the structure is not tight enough, there are gaps between the layers, resulting in a decrease in heat transfer capacity, which in turn affects the conversion of thermal energy to electricity.

4.3. Possible methods for improvements

There are several possible ways to improve the prototype. The first option is to optimize the materials used in it, enhancing heat transfer through the characteristics of the material itself. Strengthening the structural design to reduce the gap between the layers is also an option, and the closer bonding of the layers also helps to maintain heat transfer. Another possible method is to add a controllable frame to effectively track the source of heat radiation. It is also an option to combine the prototype with photovoltaic (PV) panels. The temperature of the PV panels will reach 328.15 K to 338.15 K when working [26,27]. Combining with the full day power generation solar building component, it could reduce the back-sheet temperature of the PV panel and increase the conversion of heat to electricity.

5. Conclusions

This paper presents a prototype of the low-cost full-day power generation solar building component. It can be integrated as the building fabric or as a part of the solar panels. The contributions are concluded as followings:

(1) The low-cost full-day power generation solar building component is presented. The prototype can work all day, even in rainy conditions.

(2) This research has done experiments on the prototype and tested its performance. It reaches a maximum of 10 mW/m^2 under sunlight. It can also work at night depending on the thermal radiation of the environment.

(3) In the experimental environment, the radiation heat transfer has a stronger influence on energy conversion than the convective heat transfer. When optimizing the prototype in similar environments, it is necessary to take full advantage of solar radiation.

(4) The relative humidity has certain influence on its performance, but there is no obvious effect of radiation heat transfer.

Although the prototype has great potential, there are still shortcomings, and this article also discusses the problems. Meanwhile, this article also provides possible directions for improving design in the future. The results in this article might be helpful for zero-energy buildings and low-carbon buildings.

Acknowledgments

J. Li would like to express his gratitude to the supports of Hunan Provincial Innovation Foundation for Postgraduate (No. CX20190289)

References

[1] IPCC, Global Warming of 1.5 ºC, IPCC. (2018). https://www.ipcc.ch/sr15/ (accessed May 9, 2020).

[2] IEA, 2019 Global Status Report for Buildings and Construction, 2019.

[3] IEA, Data & Statistics - IEA, (2019). https://www.iea.org/data-and-statistics?country=WORLD&fuel=Energy supply&indicator=Coal production by type (accessed September 4, 2020).

[4] Z. Ioannidis, A. Buonomano, A.K. Athienitis, T. Stathopoulos, Modeling of double skin façades integrating photovoltaic panels and automated roller shades: Analysis of the thermal and electrical performance, Energy Build. (2017). https://doi.org/10.1016/j.enbuild.2017.08.046.

[5] G. Barone, A. Buonomano, C. Forzano, G.F. Giuzio, A. Palombo, Passive and active performance assessment of building integrated hybrid solar photovoltaic/thermal collector prototypes: Energy, comfort, and economic analyses, Energy. 209 (2020) 118435. https://doi.org/10.1016/j.energy.2020.118435.

[6] X.F. Zheng, C.X. Liu, Y.Y. Yan, Q. Wang, A review of thermoelectrics research - Recent developments and potentials for sustainable and renewable energy applications, Renew. Sustain. Energy Rev. 32 (2014) 486–503. https://doi.org/10.1016/j.rser.2013.12.053.

[7] J. Deng, F. Zhou, B. Shi, J.L. Torero, H. Qi, P. Liu, S. Ge, Z. Wang, C. Chen, Waste heat recovery, utilization and evaluation of coalfield fire applying heat pipe combined thermoelectric generator in Xinjiang, China, Energy. 207 (2020) 118303. https://doi.org/10.1016/j.energy.2020.118303.

[8] H. Su, F. Zhou, H. Qi, J. Li, Design for thermoelectric power generation using subsurface coal fires, Energy. 140 (2017) 929–940. https://doi.org/10.1016/j.energy.2017.09.029.

[9] W. Ye, C. Liu, J. Liu, C. Zhao, T. Dai, K. Ma, Experimental Research of Ship Waste Heat Utilization by TEG-ORC Combined Cycle, Hsi-An Chiao Tung Ta Hsueh/Journal Xi'an Jiaotong Univ. 54 (2020) 50–57. https://doi.org/10.7652/xjtuxb202008007.

[10] M.A. Al-Nimr, W.A. Al-Ammari, M.E. Dahdolan, Utilizing the evaporative cooling to enhance the performance of a solar TEG system and to produce distilled water, Sol. Energy. (2017). https://doi.org/10.1016/j.solener.2017.02.037.

[11] U. Chiarotti, V. Moroli, F. Menchetti, R. Piancaldini, L. Bianco, A. Viotto, G. Baracchini, D. Gaspardo, F. Nazzi, M. Curti, M. Gabriele, Development of a small thermoelectric generators prototype for energy harvesting from low temperature waste heat at industrial plant, J. Nanosci. Nanotechnol. 17 (2017) 1586–1591. https://doi.org/10.1166/jnn.2017.13723.

[12] Y.S. Cheng, Y.H. Liu, S.C. Wang, B.R. Peng, Development of an 1.2 kW thermoelectric generation system for industrial waste heat recovery, in: 2017 IEEE 3rd Int. Futur. Energy Electron. Conf. ECCE Asia, IFEEC - ECCE Asia 2017, Institute of Electrical and Electronics Engineers Inc., 2017: pp. 1246–1250. https://doi.org/10.1109/IFEEC.2017.7992221.

[13] V. Abbasi, V.S. Tabar, Measurement and evaluation of produced energy by thermoelectric generator in vehicle, Meas. J. Int. Meas. Confed. 149 (2020) 107035. https://doi.org/10.1016/j.measurement.2019.107035.

[14] R. García-Contreras, A. Agudelo, A. Gómez, P. Fernández-Yáñez, O. Armas, Á. Ramos, Thermoelectric energy recovery in a light-duty diesel vehicle under real-world driving conditions at different altitudes with diesel, biodiesel and GTL fuels, Energies. (2019). https://doi.org/10.3390/en12061105.

[15] T.K. You, H. Mohamed, M. Mujaini, Experimental study on the effects of tightening on the performance of thermoelectric generator for human body heat harvesting, Int. J. Emerg. Trends Eng. Res. (2020). https://doi.org/10.30534/ijeter/2020/76852020.

[16] H.M. Elmoughni, A.K. Menon, R.M.W. Wolfe, S.K. Yee, A Textile-Integrated Polymer Thermoelectric Generator for Body Heat Harvesting, Adv. Mater. Technol. 4 (2019) 1800708. https://doi.org/10.1002/admt.201800708.

[17] M. Hyland, H. Hunter, J. Liu, E. Veety, D. Vashaee, Wearable thermoelectric generators for human body heat harvesting, Appl. Energy. 182 (2016) 518–524. https://doi.org/10.1016/j.apenergy.2016.08.150.

[18] J. Yuan, R. Zhu, Self-Powered Wearable Multi-Sensing Bracelet with Flexible Thermoelectric Power Generator, in: 2019 20th Int. Conf. Solid-State Sensors, Actuators Microsystems Eurosensors XXXIII, TRANSDUCERS 2019 EUROSENSORS XXXIII, Institute of Electrical and Electronics Engineers Inc., 2019: pp. 1431–1434. https://doi.org/10.1109/TRANSDUCERS.2019.8808231.

[19] G. Yu, H. Yang, Z. Yan, M. Kyeredey Ansah, A review of designs and performance of façade-

based building integrated photovoltaic-thermal (BIPVT) systems, Appl. Therm. Eng. 182 (2021) 116081. https://doi.org/10.1016/j.applthermaleng.2020.116081.

[20] K. Irshad, K. Habib, R. Saidur, M.W. Kareem, B.B. Saha, Study of thermoelectric and photovoltaic facade system for energy efficient building development: A review, J. Clean. Prod. 209 (2019) 1376–1395. https://doi.org/10.1016/j.jclepro.2018.09.245.

[21] L. Fan, W. Li, W. Jin, M. Orenstein, S. Fan, Maximal nighttime electrical power generation via optimal radiative cooling, Opt. Express. 28 (2020) 25460. https://doi.org/10.1364/oe.397714.

[22] A. Aksamija, Z. Aksamija, C. Counihan, D. Brown, M. Upadhyaya, Experimental study of operating conditions and integration of thermoelectric materials in facade systems, Front. Energy Res. (2019). https://doi.org/10.3389/fenrg.2019.00006.

[23] A.P. Raman, W. Li, S. Fan, Generating Light from Darkness, Joule. 3 (2019) 2679–2686. https://doi.org/10.1016/j.joule.2019.08.009.

[24] A. Rezania, L.A. Rosendahl, A comparison of micro-structured flat-plate and cross-cut heat sinks for thermoelectric generation application, Energy Convers. Manag. (2015). https://doi.org/10.1016/j.enconman.2015.05.064.

[25] F.J. Lesage, É. V. Sempels, N. Lalande-Bertrand, A study on heat transfer enhancement using flow channel inserts for thermoelectric power generation, Energy Convers. Manag. (2013). https://doi.org/10.1016/j.enconman.2013.07.002.

[26] A. Ozemoya, A. Swart, H.C. Pienaar, R. Schoeman, Factors impacting on the surface temperature of a PV panel, in: 2013.

[27] S.P. Aly, S. Ahzi, N. Barth, Effect of physical and environmental factors on the performance of a photovoltaic panel, Sol. Energy Mater. Sol. Cells. (2019). https://doi.org/10.1016/j.solmat.2019.109948.